Solar Activity Dependency of a Specular Intake for an ABEP System

Nadine Barth[1*], Jonathan Skalden[1], Konstantinos Papavramidis[1], Franziska Tuttas[1], Marcel Pfeiffer[1], Julian Beyer[1], Raphael Tietz[1], Stefanos Fasoulas[1], Georg Herdrich[1*]

[1]Institute of Space Systems, University of Stuttgart, Stuttgart, 70569, Germany.

*Corresponding author(s). E-mail(s): herdrich@irs.uni-stuttgart.de;

Abstract

Challenging space missions at very low altitudes face significant atmospheric drag, requiring efficient propulsion methods such as Atmosphere-Breathing Electric Propulsion (ABEP) to extend mission lifetimes. ABEP captures atmospheric particles and uses them as propellant for an electric thruster, reducing dependence on limited on-board propellant. This could extend missions in Very Low Earth Orbit (VLEO) and on celestial bodies with an atmosphere, such as Mars. The Institute of Space Systems (IRS), under the EU H2020 DISCOVERER, ESA Ram-CLEP, and CRC ATLAS projects, is developing a high-efficiency specular intake and a RF Helicon-based plasma thruster (IPT) for ABEP. This study uses the numerical tool PICLas and it's Direct Simulation Monte Carlo Method's (DSMC) to analyse the effect of solar activity and evaluate the validity of the hyperthermal assumption in VLEO for ABEP intake designs. Additionally, the effect of changing intake lengths on important key parameters, such as intake efficiency, mass flow rate, and pressure, is examined. The results show that efficiency decreases with higher solar activity, longer intakes and higher altitudes, with particle temperature having the greatest effect on efficiency, due to its influence on thermal velocity and the molecular speed ratio. An almost linear relationship between efficiency and molecular speed ratio is shown, revealing that the hyperthermal assumption may not be valid for VLEO applications. To achieve the required pressure level for ignition, flexible ABEP operation is recommended to accommodate for varying solar activity, suggesting lower altitude operation during low solar activity and higher altitude operation during high solar activity.

Keywords: ABEP, Intake, DSMC, Very low Earth orbit, Dynamic thermosphere

1 Introduction

1.1 ABEP Concept

Missions at Very Low Earth Orbit (VLEO), where the atmosphere causes aerodynamic drag on the spacecraft, are among the most challenging space missions. An efficient propulsion system to compensate for the drag is required to extend their lifetime. One potential solution is Atmosphere-Breathing Electric Propulsion (ABEP), which collects atmospheric particles and uses them as propellant for an electric thruster. The ABEP principle, shown in Fig. 1, consists of two main components: an intake that collects residual atmospheric particles and directs them into the discharge channel (DC) region, and an electric thruster, which accelerates these particles to generate thrust.

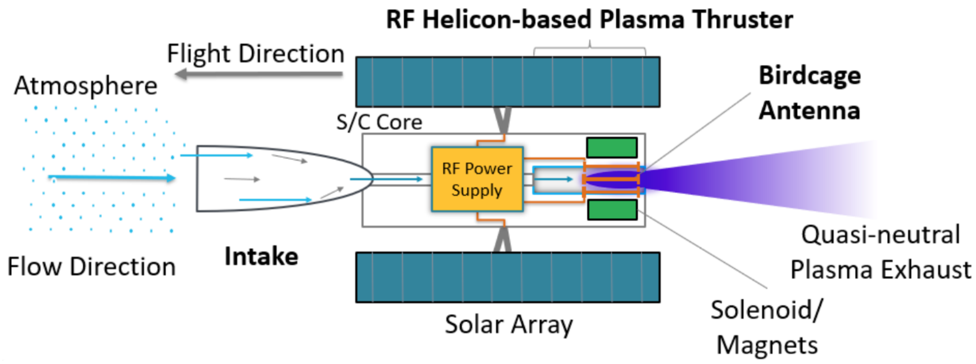

Fig. 1 ABEP schematic, showing an examplary spacecraft in VLEO collecting atmosphere with an parabolically shaped specular intake and a RF Helicon-based plasma thruster with birdcage antenna to generate thrust [1]

The system is designed to operate in VLEO below 450 km. In theory, it can be applied to any planetary body with an atmosphere, reducing the need for stored propellant and extending the lifetime of the satellite. The satellite platform and the corresponding ABEP are described in more detail by Herdrich et al [2, 3]. Broader research on realising satellite operations in VLEO is being conducted in the framework of the Collaborative Research Center (CRC) 1667 ATLAS, which is located at the University of Stuttgart and funded by the German Research Foundation DFG.

1.2 ABEP Intake Key Parameters

The ABEP system intake is designed to collect atmospheric particles and channel them into the DC of the thruster. The key parameters of an ABEP intake are the collection efficiency, as well as pressure and mass flow rate to ensure adequate thruster operation, while minimising its area and volume.

The collection efficiency η_c is a key parameter to evaluate the ABEP intake and is defined in Eq. (1), by dividing the collected particle flux at the DC outlet $\dot{N}_{out}$ by the incoming particle flux $\dot{N}_{in}$:

$$\eta_c = \frac{\sum_{i=1}^{N_s} \dot{N}_{out_i}}{\sum_{i=1}^{N_s} \dot{N}_{in_i}}. \tag{1}$$

The incoming particle flux $\dot{N}_{in}$ is thereby calculated by particles passing through a reference area as big as the size of the intake area. N_s represents the total number of species present in the atmospheric environment. In this work, seven different atmospheric species are considered: O (in this paper also referred to as AO), N_2, O_2, He, Ar, H, N. The flow environment for ABEP calculations, namely density, temperature, and velocity, is particularly challenging as it varies considerably with altitude, solar dynamics and orbit configuration.

Another important key parameter is the pressure in the DC p_{DC}, as the pressure must be high enough to ignite the thruster. It is calculated using n as the particle number density, k_b as the Boltzmann constant and T as the particle temperature by applying the ideal gas law in Eq. (2):

$$p_{DC} = \sum_{i=1}^{N_s} n_i k_b T_i. \tag{2}$$

The particle densities vary for different species, while the temperature of the particles is assumed to be at equilibrium.

The last key parameter is the mass flow rate into the DC $\dot{m}_{DC}$, which is dependent on the particle mass m and the particle flux:

$$\dot{m}_{DC} = \sum_{i=1}^{N_s} m_i \cdot \dot{N}_{out_i}. \tag{3}$$

1.3 Intake Literature Review

The development of ABEP intakes began in 2003 with JAXA's design of ABIE, the first diffuse intake for an ABEP system [4]. The University of Colorado later conducted the first examination of a specular intake design in 2018 [5]. Since then, numerous intakes have been developed, both in hardware and in conceptual design, including both diffuse and specular designs by IRS [6]. An overview of previous intake systems is given in Table 1. Jianjun and Zheng [33] have also recently provided a comprehensive review of ABEP intake designs.

However, this paper does not examine the details of the in Table 1 mentioned diffuse intake designs, as it focuses on specular intake designs, which are discussed in more detail subsequently.

The University of Colorado evaluated three different types of specular intake shapes: pyramidal, conical and parabolic. Their results show that under ideal specular reflection conditions, the parabolic shape outperforms the other two due to the optics

Table 1 Literature overview over ABEP Intake systems

Institution	Design	Year	Scattering	η_c	References
JAXA	ABIE	2003	Diffuse	0.28-0.46	[4, 7–11]
ESA	RAM-EP	2007	Diffuse	-	[12]
BUSEK	MABHET	2012	Diffuse	0.2-0.4	[13]
SITAEL, VKI	RAM-EP	2015	Diffuse	0.28-0.32	[14–20]
Lanzhou Inst.	Hybrid system (active)	2015	Diffuse	0.42-0.58	[21]
IRS	EFD	2016	Diffuse	0.458	[22, 23]
TsAGI	Air-breathing ion engine	2017	Diffuse	0.33-0.34	[24–29]
University of Colorado	ABEP for CubeSat Applications	2018	Specular	>0.9	[5]
IRS	Specular	2021	Specular	0.943	[3, 6, 30]
Zheng	ABEP for 3U Cubesat	2023	Specular/ Diffuse	0.61-0.63	[31]
Sannino	DSMC comparison between different GSI models (CLL and Maxwell)	2025	Specular/ Diffuse	0.979	[32]

of a parabolic mirror, which reflects all incident particles to the focal point of the parabola. By utilising the optical properties of a parabola, the final design achieved a simulated collection efficiency of $\eta_c > 90\%$.

Zheng et al. [31] investigated a hybrid intake design combining specular and diffuse elements. They investigated a fully specular parabolic intake with additional honeycomb ducts, typical of diffuse intakes, and achieved a simulated collection efficiency of $\eta_c = 63.5\%$.

Recently, Sannino [32] published a study comparing different Gas-Surface Interaction (GSI) models, specifically the Maxwell and Cercignani-Lampis-Lord (CLL) model [34], considering a wide range of possible material reflection patterns. In the fully specular and fully diffusive case, the two GSI models showed similar results.

At IRS, Romano conducted simulations comparing diffuse and specular intake designs, including a combination of both [6]. He optimised the specular design for the optimal focal point position, achieving efficiencies up to $\eta_c = 94\%$, outperforming the other designs. The promising results from Romano's specular intake design have been further investigated at the IRS [3, 30] and in this paper.

2 Theoretical Description

2.1 Rarified Flow

The Navier-Stokes equations, which are valid for fluid dynamics in the continuum regime on Earth, lose their validity at high Knudsen numbers above $0.1 - 0.25$. In the very low-density regime of VLEO, where the mean free path exceeds the characteristic length, these equations are no longer applicable. Depending on the Knudsen number, the flow is typically classified as either transitional ($0.1 < \mathrm{Kn} < 10$) or free molecular flow regime ($\mathrm{Kn} > 10$). Additional flow conditions in VLEO require the consideration of collisions, which requires solving the Boltzmann equations. [35]

In addition to a low number of collisions in free molecular flow, an essential parameter is the molecular speed ratio s. This ratio describes the relationship between the

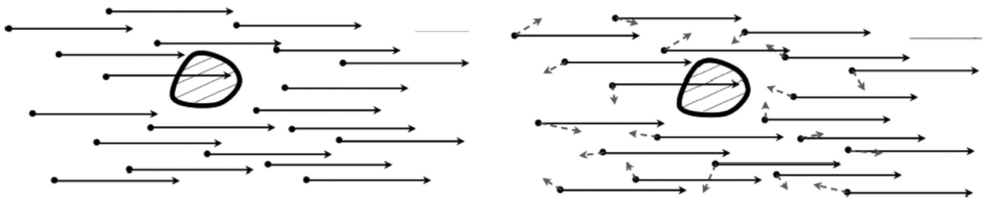

(a) Hyperthermal (b) Hypothermal

Fig. 2 Illustration of hyperthermal and hypothermal flow conditions according to Prieto [35]

bulk velocity of the collimated beam v_{m} and the thermal velocity of the particles v_{th}:

$$s = \frac{v_{\mathrm{m}}}{v_{\mathrm{th}}}. \tag{4}$$

The molecular speed ratio is a measure of whether the flow can be classified as hyperthermal or hypothermal. In a hyperthermal flow, the molecules behave like a collimated beam, whereas in a hypothermal flow they exhibit the characteristics of a drifting Maxwellian flow, with particles having higher thermal velocities. Fig. 2 illustrates the hyperthermal and hypothermal flow in an illustration according to Prieto [35].

Typically, a flow is considered hyperthermal for $s > 5$ and hypothermal for $s < 5$. However, in nature there is no clear boundary as the transition is gradual. This assumption must be re-evaluated for each specific application. In the case of specular intake design, even small deviations in the angle of the particle trajectories can lead to significant variations in the overall results.

Using the kinetic theory of gases and the Boltzmann distribution, it can be shown that the mean thermal velocity v_{th} can be calculated using the following Eq.:

$$v_{\mathrm{th}} = \sqrt{\frac{8 k_{\mathrm{b}} T}{\pi m}}. \tag{5}$$

It can be seen that an increase in particle temperature leads to an increase in thermal velocity, which increases the spread of the angles of the particle trajectories. This can be observed on the right in Fig. 2 if both arrows are combined to one final trajectory for each particle. Additionally, particle mass plays a critical role, as lighter species have higher thermal velocities and are therefore more likely to not fulfill the assumption of hyperthermality.

2.2 Gas-Surface Interaction

As previously mentioned, in VLEO the free molecular flow regime is typically characterised by a low number of collisions, highlighting the significant influence of particle-wall interactions. Therefore, accurate modelling of particle surface interactions is crucial in this flow regime and essential for the intake design. In general, particles can be absorbed, scattered or undergo chemical reactions on surfaces [36].

Unfortunately accurate modelling of these processes is highly complex due to insufficient knowledge of surface properties such as surface finish, cleanliness, and adsorbed gas layers, especially in the VLEO environment where interactions with various gases, especially atomic oxygen (AO), are significant.

The Maxwell model is a simplified, but well-established state-of-the-art approach that considers two types of surface-particle interaction: specular and diffuse reflection. The schemes are shown in Fig. 3. [36]

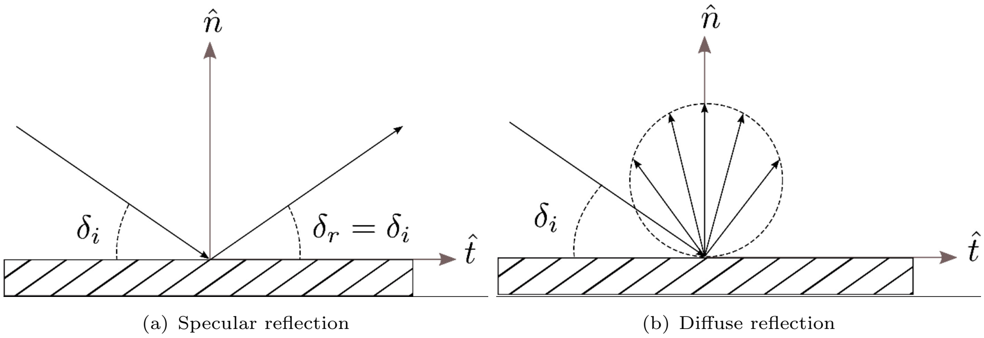

Fig. 3 Mechanisms of re-emission for specular reflection without thermal accommodation and diffuse reflection with complete thermal accommodation [36]

The incoming particle velocity is indicated by the arrow, the vectors $\widehat{n}$ and $\widehat{t}$ are the normal and tangential unit vectors, and δ_i and δ_r are the incident and re-emission angles, respectively. For specular reflection (left), the particles are reflected in an angle $\delta_\mathrm{r} = \delta_\mathrm{i}$, with no energy exchange, and the tangential component of the particle velocity remains constant. For a diffuse reflection (right), the reflected particle velocity is completely independent of the incident particle velocity and direction. After hitting the surface, the particles reach thermal equilibrium with the surface and are reflected: parallel to the surface according to a Rayleigh distribution and normal to the surface according to a Maxwell-Boltzmann distribution, corresponding to the wall temperature T_W. The type of scattering that takes place is primarily a function of the surface material.

The Maxwell model defines the accommodation coefficient α, as shown in Eq. (6):

$$\alpha = \frac{E - E'}{E - E_\mathrm{W}}. \tag{6}$$

Here, E is the particle energy, E' is the reflected particle energy, and E_W is the energy of full accommodation to the wall. A fully diffuse reflection corresponds to $\alpha = 1$, while a fully specular reflection corresponds to $\alpha = 0$. The intakes currently under development can equally be grouped in the two categories: "diffuse" and "specular", depending on which reflection/re-emission mechanism their design relies on.

While the Maxwell model is widely used due to its simplicity and engineering relevance, more advanced gas-surface interaction models, such as the CLL model [34], offer improved physical accuracy by independently accounting for normal and tangential momentum and energy accommodation. However, the implementation of the CLL model requires detailed, material-specific parameters, which are not yet available for the surfaces considered in this study. Since the current work focuses on a comparative analysis of fully specular intake designs, and results for both fully diffuse and fully specular designs are identical for both models [32], the Maxwell model was chosen and is subsequently used to describe the interactions between particles and surfaces.

2.3 Intake Material

The effectiveness of the overall system depends heavily on the careful selection of the intake materials, as gas-surface interactions have a significant impact on the system's ability to capture atmospheric particles and deliver them to the electric thruster. In addition, the chosen material must have sufficient resistance to AO exposure, be lightweight for satellite applications, and non-magnetic to avoid interference with the flow environment generated in ground test facilities. According to Murray [37] Silica (SiO_2) emerges as promosing candiate material due to its commendable chemical and thermal stability, coupled with good specular reflection properties. Another material is highly oriented pyrolytic graphite (HOPG), known for its narrow angular distribution and potentially superspecular characteristics. HOPG demonstrates commendable inertness with O_2 at low surface temperatures and minimal reactivity with atomic oxygen, which is promising in terms of the intake material's degradation. However, the current challenges in manufacturing make a HOPG intake both intricate and costly, necessitating a careful trade-off.

A plausible alternative is to apply a SiO_2 plasma-based coating to the intake. A silicon carbide (SiC) passivation is being considered to provide a basis for a thorough evaluation of SiO_2 as an intake coating material. As a result of its expertise, IRS may be in a position to carry out the SiC passivation [38, 39]. The anticipated surface smoothness for the SiO_2 coating is at least 0.94 Å, as previously used by Murray [37].

3 Methodology

3.1 Specular Intake Design at IRS

Flow in VLEO is typically treated as hyperthermal, with particles primarily moving parallel to the spacecraft velocity vector. This behavior allows for optical principles to be applied, making a parabolic shape, similar to that of parabolic mirrors, particularly effective. The parabolic shape efficiently directs incoming particles to the focal point of the paraboloid. When interacting with the surface, the particles retain their tangential velocity component, while their normal velocity component is reversed without energy exchange. This hypothesis relies on the assumption of hyperthermal flow. However, as discussed in section 2.1, the validity of this assumption will be examined in this paper.

The used paraboloid for the specular intake is characterized by its focal point F and its distance between it and the vertex named focal length f. Additionally its intake frontal diameter d_{In}, its parabola length l_{In}, as well as the DC diameter d_{DC} play a critical role. All geometric parameters are shown in Fig. 4.

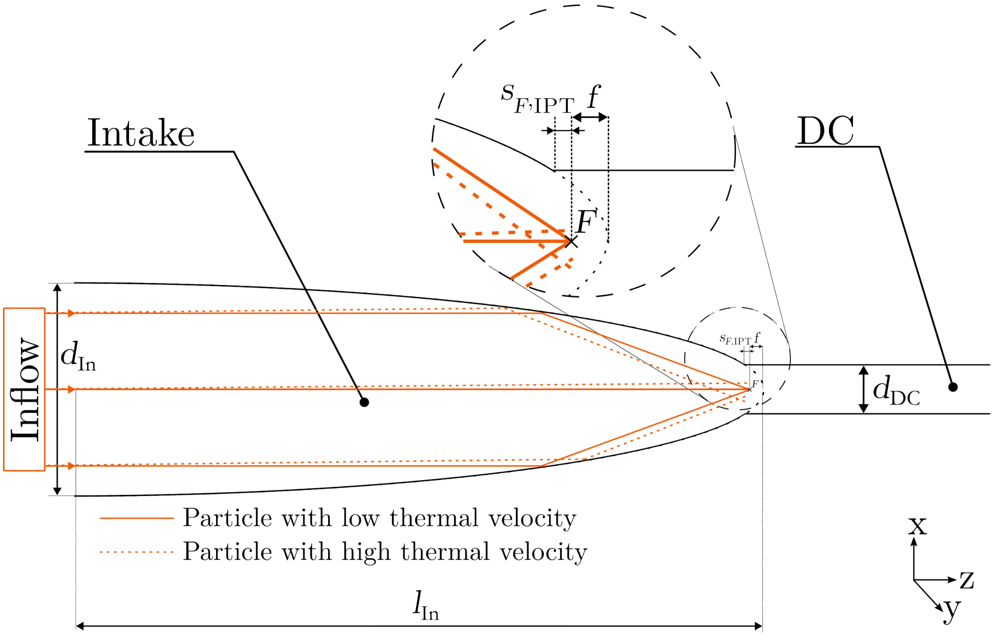

Fig. 4 Functional schematic of the paraboloid, showing the focus point position inside the discharge channel and example trajectories of particles with high and low thermal velocity

The shape of the paraboloid is determined by the focal length f, which in turn depends on the diameter of the thruster's discharge channel. Romano [6] has shown that the position of the focal point - whether inside, outside or exactly at the entrance plane of the discharge channel - has a significant effect on the collection efficiency, with a focal point inside the discharge channel resulting in the highest collection efficiency.

Additionally, Fig. 4 shows that particles with low thermal velocities are perfectly reflected into the focal point. In contrast, particles with higher thermal velocities experience a slight deviation in their trajectory angle, making it less likely that they will be precisely focused to the focal point.

In this study, a parabola with a DC diameter of $d_{\mathrm{DC}} = 37\,\mathrm{mm}$ with varying intake length is considered. The DC diameter is derived from the thruster's diameter, which, in case of IRS, is 37 mm [6]. Additionally a SiC intake with a SiO_2 coated inner surface is assumed with a specularity of 100%.

There are two critical assumptions that need to be carefully considered in the design of future specular intakes. The first is the aforementioned assumption of 100% specularity, as no material currently achieves this level of specularity. Romano [6] investigated this issue and found that even a 20% reduction in specularity outperformed diffuse intake designs under similar atmospheric conditions. Later in this paper, this assumption will be examined in detail, and a reduction up to 50% specularity will be analyzed.

The second critical assumption relates to the assumption of hyperthermal flow, where the molecules are considered as a collimated beam. The choice of the parabolic shape for the intake is mainly based on this assumption. This assumption has proved effective for low solar activity levels in previous studies [6]. However, the consideration of higher solar activity leads to higher temperatures and consequently higher thermal velocities and an increased molecular speed ratio s, which requires a more detailed investigation, which is carried out in this paper.

3.2 Atmospheric Modeling

Several models can be used to simulate the atmosphere. The NRLMSISE-00 model [40] has become the standard in international space research and is preferred for its accurate representation of lower thermospheric conditions. It has also been used in previous ABEP system research [6, 30].

Previous studies at IRS have used atmospheric data for a specific day when atmospheric activity was very low. This study will compare the results at different levels of atmospheric activity. The ISO-14222 [41] and ECSS [42] standards define the levels of atmospheric activity, as shown in Table 2.

Table 2 Solar cycle 23 atmospheric data from ECSS [42]

	Long-term (>27 days)			Short-term (daily)		
	Low	Moderate	High	Low	Moderate	High
$F10.7$	65	140	250	65	140	300
A_p	0	15	45	0	15	240

The low and moderate conditions are identical for the short and long-term scenarios. Consequently, the following analysis examines four different conditions: low solar activity conditions, moderate solar activity conditions, long-term high solar activity conditions and short-term high solar activity conditions.

The $F10.7$ and A_p indices are used as input to the NRLMSISE-00 atmospheric model. Additional information required by the NRLMSISE-00 model includes the day of the year and time of day. However, no significant change was found in the data averaged over a year of low solar activity (2009), a year of high solar activity (2014), or the full solar cycle (2009-2019), when considering the input data of $F10.7$ and A_p. The time of day also has little effect. Therefore, the averaged data from one year was used for this study. In addition, longitude and latitude are averaged between -180° and 160° in steps of 20°, and between -90° and 90° in steps of 10°.

This study considers altitudes between 150 km and 250 km. As previously noted by Romano [6], the lower limit of 150 km is set due to an increase in drag, which increases the power requirements for the thruster and the heating of the spacecraft. While the upper limit is not fixed, it becomes increasingly difficult to collect enough particles to operate the thruster with increasing altitude at an adequate level of specific impulse. In addition, pressure will be a major challenge for high altitude operation, as a certain pressure level is required to ignite the thruster of the ABEP system. In this study, the minimum pressure level will be assumed to be 0.1 Pa, based on experiments conducted

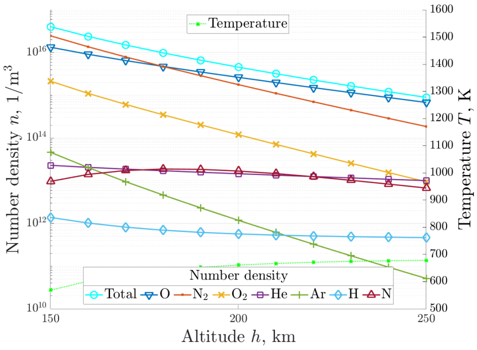

(a) Low conditions

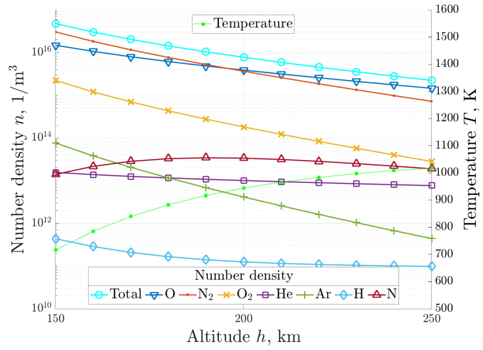

(b) Moderate conditions

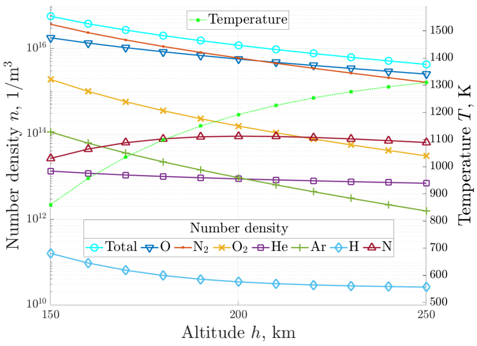

(c) Long-term high conditions

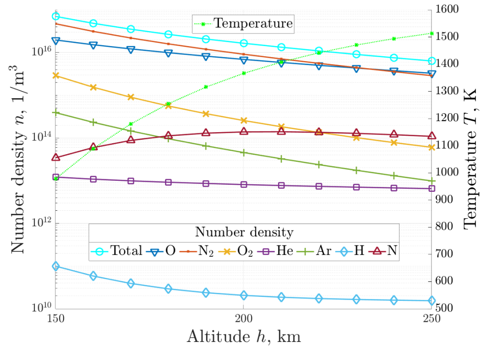

(d) Short-term high conditions

Fig. 5 Atmospheric conditions of moderate, long-term high and short-term high conditions, showing the number density of specific species, total density and temperature at different altitudes

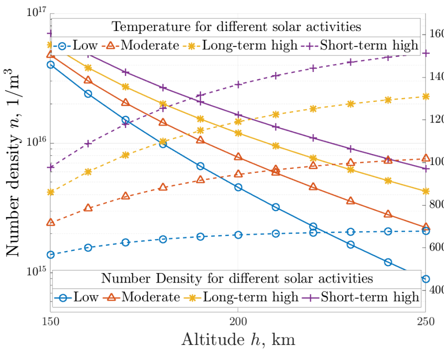

(a) Comparison of number density and temperature

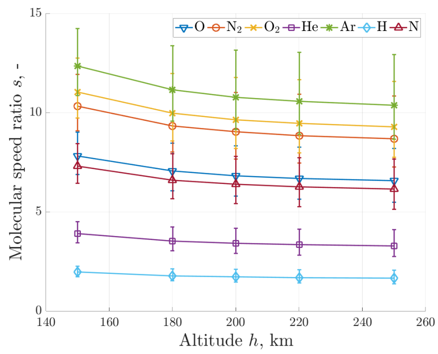

(b) Molecular speed ratio for different species

Fig. 6 Comparison of total number density, temperature for all considered atmospheric conditions (left) and molecular speed ratio range over different atmospheric conditions (right) for different species with the ABEP IPT at this pressure level [3]. A lower threshold pressure could be required.

Figure 5 shows the detailed atmospheric conditions with the 7 species considered, the total number density as well as the temperature for all four considered atmospheric condition. In all cases, the dominant species are N_2 and AO. A comparison of all the total number density, as well as the temperatures over different altitudes is shown on the left in Fig. 6.

The particle density in all plots is presented on a logarithmic scale to better show the decrease with increasing altitude. It can be seen that the density changes by a factor of 10 for different altitudes, while the different solar activity levels have a smaller influence when the altitude is kept constant.

For temperature, on the other hand, altitude has a smaller effect than solar activity levels, which also results in a much higher thermal velocity. This suggests that while changes in density are more sensitive to changes in altitude, changes in temperature are more influenced by variations in solar activity.

The particle velocity is assumed to correspond to orbital velocity, which varies slightly with altitude, ranging from approximately 7814 m/s at 150 km to 7754 m/s at 250 km. To further characterize the flow regime, the Knudsen number is calculated using collision cross-section from Bird [43] and the largest characteristic length considered in this study, $\mathrm{L} = 1.5\,\mathrm{m}$. The resulting free-stream Knudsen numbers are > 25, confirming that the flow lies deep in the rarefied regime across all cases considered.

The previously introduced molecular speed ratio, displayed on the right in Fig. 6, is calculated based on these atmospheric conditions using Eq. (4) and Eq. (5). The velocity of the collimated beam v_m, required for the calculation, is also given by the atmospheric model and does not vary much. The error bars indicate the range of the molecular speed ratio for different species across different atmospheric conditions (with the highest molecular speed ratio indicating low solar activities).

While typically a molecular speed ratio of $s = 5$ is used as a reference threshold between hyperthermal and hypothermal flow, this boundary is not sharply defined. Instead, the transition between the two regimes is gradual and depends on the specific species and atmospheric conditions. The mean molecular speed ratio lies above this boundary, which is why this regime was previously considered as hyperthermal in simulations. In Fig. 6, it can be observed, that for some of the species namely H and He the molecular speed ratio lies below this threshold, while heavier species such as N and O approach $s = 5$ particularly under higher temperature conditions. This indicates that the flow conditions do not uniformly fall within a single regime, and therefore, the assumption of a purely hyperthermal regime is critically re-examined in this study.

Additionally it can be observed, that contrary to the expected increase in molecular speed ratio at higher altitudes, the molecular speed ratio gradually decreases. This effect arises from the increase in temperature at high altitudes and persists with further temperature increases and therefore altitude. Consequently, the flow regime in even higher altitude cannot be considered hyperthermal, necessitating the consideration of thermal velocity for all VLEO conditions. Therefore, PICLas is used for particle simulations as it accounts for the thermal velocity of particles.

3.3 Flow Field Simulations with PICLas

For rarefied gas conditions, the assumptions behind the Navier-Stokes equations are no longer valid. Therefore, the ABEP intake simulations presented in this work are conducted using the Direct Simulation Monte Carlo (DSMC) method, rather than continuum simulation methods such as Computational Fluid Dynamics (CFD).

The three-dimensional, open-source particle code PICLas [44] is used for these simulations. PICLas approximates the integro-differential Boltzmann equation by coupling various particle methods for the modelling of non-equilibrium and reactive gas and plasma flows. In this study, only the DSMC method implemented in PICLas is used. PICLas is developed in collaboration between the Institute of Space Systems (IRS) at the University of Stuttgart and the spin-off company boltzplatz numerical plasma dynamics GmbH.

The DSMC method, originally introduced by Bird [43], is a probabilistic approach that models the particle distribution function using weighted simulation particles. It separates particle motion and collisions in discrete steps and samples macroscopic quantities such as density and temperature from the statistical behaviour of the particles. Interparticle collisions, which involve interactions between different simulation particles, are fully accounted for in the method, ensuring a more realistic representation of gas dynamics.

A statistical pairing algorithm randomly pairs particles within each cell. The implemented octree algorithm in PICLas [45] refines a cell recursively until the mean free path is resolved. For all simulations, the number of particles per cell was kept above 50 to ensure sufficient statistical sampling. The time steps and particle weighting factors were selected such that both the mean free path and the local collision frequency were adequately resolved. The Variable Hard Sphere (VHS) model is used for collision dynamics, which is commonly applied in rarefied gas simulations. VHS species parameters can be found in Bird [43]. An overview of the main simulation parameters used in PICLas is shown in Table 3.

Table 3 Key parameters used in the DSMC simulation setup with PICLas.

Collision model	Variable Hard Sphere (VHS)
Time step	2×10^{-7} s
Particle weighting factor	1×10^{8} or 1×10^{9}
Maximum collision probability per time step	< 0.1
Particles per cell	> 50

The rotational symmetry of the intake allows for a two-dimensional axisymmetric simulation approach in PICLas, which significantly reduces computational cost. The varying simulation conditions include altitude, solar activity level, and intake geometry, and are summarized in Table 4.

The results are averaged across the full DC radius at a z-position of 164 mm downstream of the intersection between the intake and the DC.

It is important to note that most of the simulations assume a specularity of 100% using the previously introduced Maxwell model as the gas-surface interaction model.

Table 4 Varying input parameters for the 2D axisymmetric DSMC simulations in PICLas.

Altitudes	$h = \{150\,\text{km}, 180\,\text{km}, 200\,\text{km}, 220\,\text{km}, 250\,\text{km}\}$
Solar activity levels	Low, moderate, long-term high, and short-term high solar activity (deciding free stream temperature, velocity and particle number density)
Free stream temperatures	568 K to 1513 K (see Fig. 6a)
Free stream velocities	7754 m/s to 7814 m/s
Free stream particle densities	8.9×10^{14} to $7.0 \times 10^{16}\,\text{m}^{-3}$ (see Fig. 6a)
Intake lengths and diameters	$l_{\text{in}} = \{500\,\text{mm}, 1000\,\text{mm}, 1500\,\text{mm}\}$ $d_{\text{in}} = \{210\,\text{mm}, 296\,\text{mm}, 364\,\text{mm}\}$

This assumption represents an idealized condition that has not yet been achieved in practical applications. A decrease in specularity is expected to correspond to a decrease in intake efficiency, as demonstrated by Romano [6] for low atmospheric conditions. The assumption was made to assess the influence of the solar activity level on the varying specularity level and will be reevaluated in chapter 4.6.

4 Simulation Results and Discussion

4.1 Radial Non-Uniformity

For all simulations it was observed that the collected particles are concentrated in the center of the DC, which is likely a result of increased particle interactions due to higher density. This results in a radial non-uniform distribution towards the channel wall and can be observed in Fig. 7. The upper part of the figure shows the total number density distribution, while the lower part shows the pressure. The effect of concentrating all particles towards the center of the channel can also be called "beaming effect" [46] and was observed in all simulations performed and also in previous conducted studies [6, 30]. No further analysis of this effect is performed. The pressure on the other hand shows the compression of the atmospheric particles to a higher pressure level, which will be discussed later on.

4.2 Simulations over Different Atmospheric Conditions

The simulation results for different atmospheric conditions are shown in Table 5. The data include observations at three different altitudes: 150 km, 200 km and 250 km, across all observed atmospheric conditions. The table presents the particle flux at both the intake inlet and the intake exit, which also serves as the inlet to the thruster/DC. The particle flux is radially integrated over the DC cross-sectional area and calculated locally for each mesh element using:

$$\dot{N}_i = nvA_i, \qquad \dot{N} = \sum \dot{N}_i, \tag{7}$$

where $\dot{N}_i$ is the local flux through the mesh element i, n is the number density, v is the velocity, and A_i is the area of the mesh element. The total particle flux $\dot{N}$ is then obtained by summing over all elements.

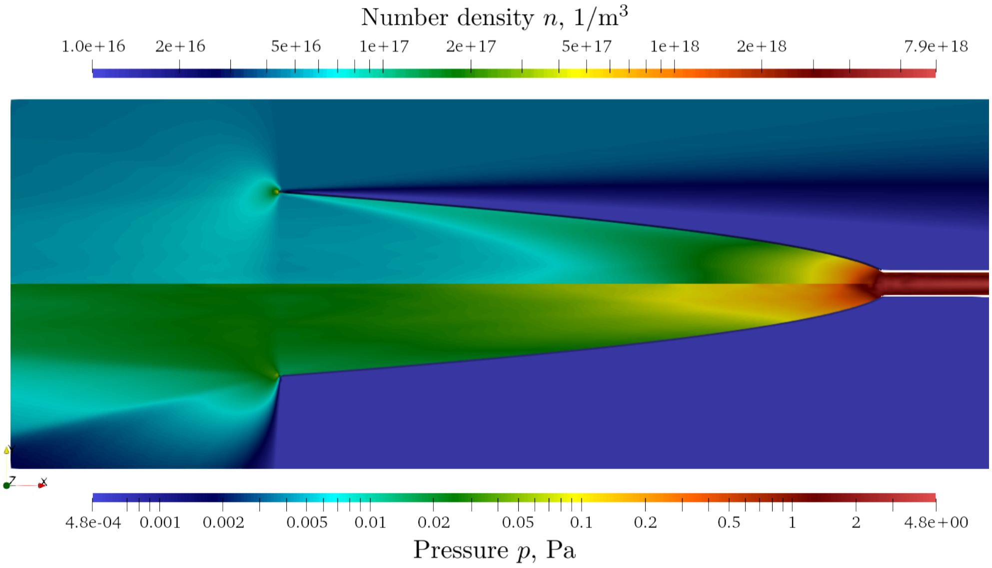

Fig. 7 Number Density (upper) and pressure (lower) results of a simulation with 1000 mm intake length with low solar activity at 150 km altitude

From these values, the collection efficiency is computed according to Equation 1. In addition, the table includes the corresponding mean and maximum pressures (Eq. 2), and mass flow rates (Eq. 3). The maximum pressure refers to the value along the centerline of the DC, where it is elevated due to the previously discussed beaming effect. The mean pressure represents the average pressure across the DC radius.

Table 5 Altitude h, molecular speed radio s, particle flux at the inlet $\dot{N}_{\mathrm{in}}$ and thruster side $\dot{N}_{\mathrm{out}}$, intake efficiency η_{c}, mass flow rate $\dot{m}_{\mathrm{out}}$ and, maximum and mean pressure p_{max}, p_{mean} simulation results of a fixed intake length of $l_{\mathrm{In}} = 500$ mm for four different atmospheric conditions at altitudes of 150 km, 200 km and 250 km

	h km	s_{mean} -	$\dot{N}_{\mathrm{in}}$ 1/(m^{2}s)	$\dot{N}_{\mathrm{out}}$ 1/(m^{2}s)	η_{c} -	$\dot{m}_{\mathrm{out}}$ mg/s	p_{max} Pa	p_{mean} Pa
low	150	11.0	$1.09{\cdot}10^{19}$	$1.03{\cdot}10^{19}$	0.943	0.417	2.490	0.774
moderate	150	9.8	$1.29{\cdot}10^{19}$	$1.17{\cdot}10^{19}$	0.912	0.482	3.073	0.975
long-term high	150	9.0	$1.54{\cdot}10^{19}$	$1.35{\cdot}10^{19}$	0.879	0.556	3.663	1.186
short-term high	150	8.5	$1.90{\cdot}10^{19}$	$1.63{\cdot}10^{19}$	0.856	0.681	4.490	1.487
low	200	9.4	$1.23{\cdot}10^{18}$	$1.11{\cdot}10^{18}$	0.904	0.039	0.282	0.085
moderate	200	8.1	$2.09{\cdot}10^{18}$	$1.76{\cdot}10^{18}$	0.844	0.066	0.525	0.160
long-term high	200	7.2	$3.21{\cdot}10^{18}$	$2.54{\cdot}10^{18}$	0.791	0.096	0.807	0.249
short-term high	200	6.8	$4.44{\cdot}10^{18}$	$3.39{\cdot}10^{18}$	0.763	0.133	1.121	0.349
low	250	8.7	$2.39{\cdot}10^{17}$	$2.10{\cdot}10^{17}$	0.877	0.007	0.051	0.015
moderate	250	7.4	$5.99{\cdot}10^{17}$	$4.82{\cdot}10^{17}$	0.805	0.016	0.139	0.042
long-term high	250	6.6	$1.14{\cdot}10^{18}$	$8.50{\cdot}10^{17}$	0.747	0.030	0.265	0.082
short-term high	250	6.3	$1.70{\cdot}10^{18}$	$1.22{\cdot}10^{18}$	0.718	0.045	0.413	0.127

Comparing the intake efficiencies at a constant altitude, there is a noticeable drop in efficiency with increasing solar activity, from 94.3% to 85.6% for 150 km. This decrease is most likely caused by the increase in atmospheric temperature and the consequent increase in thermal velocity of the particles, which leads to a greater range of the angles of the particle velocities. Due to this misalignment, the particles are not reflected directly to the focal point and miss it by an increasing distance. Thus, fewer particles are collected by the intake. This effect can also be observed in Fig. 4 and is a result of the decreasing molecular speed ratio s, thus the flow can not be treated as a collimated beam anymore. This effect is amplified at higher altitudes where temperatures are higher. Thus, the efficiency drop becomes more significant at different solar activity levels, as can be seen by comparing the 150 km data with the 250 km data. The efficiency drop is only 8.7% for 150 km, while it rises to 15.9% for 250 km.

However, it is also noteworthy that despite the decrease in intake efficiency, the number of particles at the intake outlet - and consequently the mass flow rate and pressure - increase with higher solar activity due to the increase in particle density. This, on the other hand, leads to an increase in drag, requiring greater thrust compensation from the propulsion system.

Furthermore, it is important to note that all intake efficiency values obtained in this study exceed the highest simulated performance of a diffuse intake design, which was reported as 46 % [22]. As of now, this represents the highest intake efficiency observed for a fully diffuse intake under low atmospheric conditions, providing a benchmark for future performance comparisons. While the geometry analyzed in Ref. [22] differs from the parabolic design examined in this study, it represents a typical diffuse intake concept. This comparison is made deliberately to show the advantages of a fully specular intake design, as demonstrated by Herdrich [3], even under conditions of high thermal velocity.

The data in Table 5 corresponds to an intake length of $l_{\mathrm{In}} = 500\,\mathrm{mm}$. To provide a more comprehensive view, Fig. 8 illustrates simulation results across a range of intake lengths, atmospheric conditions, and altitudes. This visualization allows a comprehensive comparison of (a) efficiency and (b) mass flow rate across different parameters. The best acquired efficiency result for a fully diffuse intake is depicted as a dashed line in Fig. 8 (a).

It is evident that shorter intake lengths and lower solar activity give the highest intake efficiencies at all investigated altitudes. Furthermore, the efficiency decreases not only at higher altitudes but also at increased intake lengths. A comparison of intake efficiencies between the 500 mm and 1500 mm intake lengths show a decrease of up to 30% at low solar activity and 33% at high solar activity. This result comes from the earlier mentioned change in particle trajectory caused by higher thermal velocity, as shown in Fig. 4.

Despite the variation in intake efficiencies across the data obtained, all results for intake length of 500 mm or 1000 mm indicate higher intake efficiencies compared to the maximum achieved with diffuse intake systems. This suggests that, as long as the intake length does not exceed 1000 mm in the configuration presented in this paper, a specular parabolic intake continues to outperform diffuse intake designs.

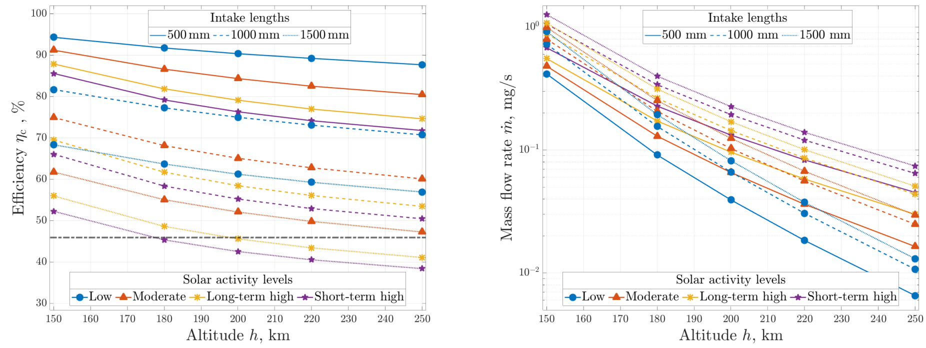

(a) Efficiency (b) Massflow

Fig. 8 Efficiency and mass flow rate for three different intake lengths and four different atmospheric conditions over altitude, with the black line showing the current efficiency limit for diffuse intakes

The right side of Fig. 8 shows the mass flow rate for all observed cases. It can be seen that the mass flow rate is higher at lower altitudes and decreases rapidly at higher altitudes. The trend of the mass flow rate calculated using Eq. (3) shows that the incoming number density (shown on the left in Fig. 6) has the strongest influence on it, as expected.

4.3 Pressure for Thruster Ignition

After comparing intake efficiency, another key parameter to consider is pressure, as the pressure within the DC plays a critical role in igniting the RF Helicon-based plasma thruster (IPT).

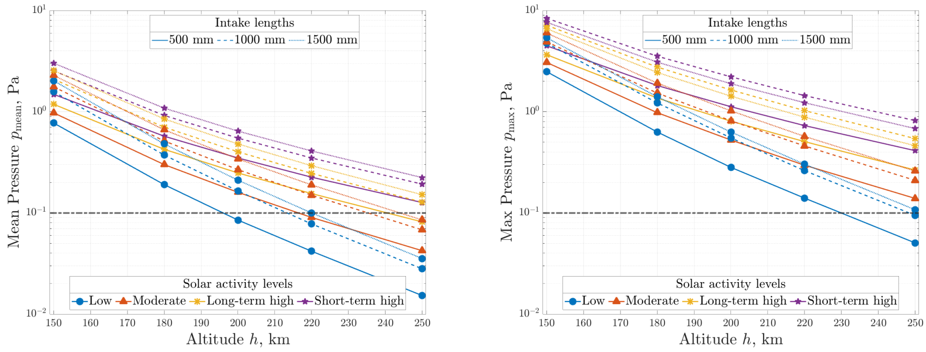

(a) Mean Pressure (b) Max Pressure

Fig. 9 Comparison of mean (left) and maximum (right) pressure results for three different intake lengths and four different atmospheric conditions over altitude, with the black line showing the required pressure for ignition of the thruster

Figure 9 shows the mean pressure over the DC (a) and the maximum pressure at the DC (b). The black line indicates a pressure level of 0.1 Pa, which has been successfully tested for the ignition of the RF Helicon-based plasma thruster [3]. Lower levels of pressure could also be sufficient, but due to a lack of experimental data, the minimum pressure level will be assumed to be 0.1 Pa. It remains uncertain whether the mean DC pressure is sufficient to ignite the thruster or whether the maximum pressure must be reached. Therefore, both pressure levels are presented here. To be conservative, it is assumed that the mean pressure of 0.1 Pa is required for ignition [6].

Figure 9 (a) clearly shows that in all cases the ignition pressure can be reached at altitudes of 150 km and 180 km. However, at higher altitudes, lower solar activity and shorter intake lengths may result in pressures below the ignition threshold. During periods of high solar activity, the ignition pressure is almost consistently achieved, except for the 500 mm intake during periods of long-term high solar activity.

If the maximum pressure inside the DC is sufficient to ignite the thruster, then the ignition pressure will be reached at every investigated altitude except at 250 km during low solar activity.

In addition to the direct pressure level, it is important to examine how the pressure ratio of the DC pressure over ambient pressure varies with solar activity, as shown in Fig. 10. This variation is influenced not only by changes in solar activity but also by intake length.

During periods of low solar activity, the pressure ratio can reach a maximum of 6400 for the largest intake length, with values ranging between 1800 and 6400 depending on the altitude. For higher levels of solar activity, the pressure ratio is reduced, with the minimum pressure ratio across the investigated altitudes around a value of 1000. The influence of intake length is highest during low solar activity, whereas its effect diminishes as the molecular speed ratio s increases.

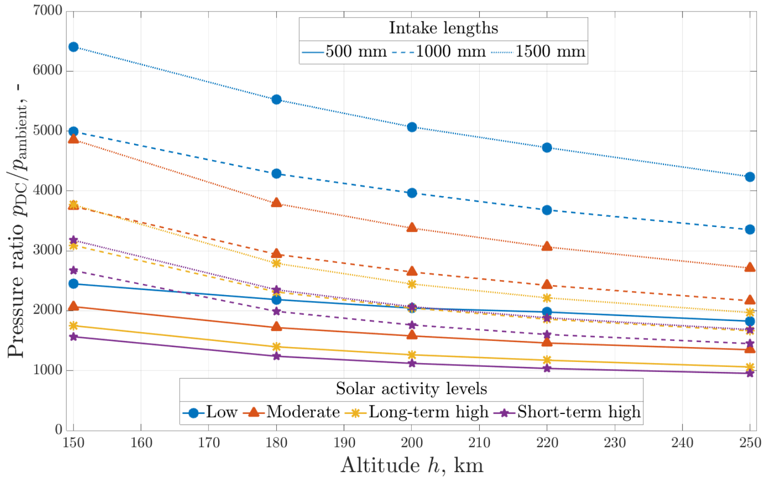

Fig. 10 Pressure Ratio of mean pressure in DC over ambient pressure for different intake lengths and solar activity levels

It is clear that pressure plays a critical role in ABEP design, with lower intake length enhancing intake efficiency but lowering pressure ratio. Maintaining ignition pressure is critical to ensure flexible operation, which is why future studies should focus on improving the ignition pressure. For now it is worth considering to allow operation in lower orbits during periods of low solar activity and therefore less drag, and operation at higher altitudes during higher solar activity and higher drag, provided it aligns with mission requirements.

4.4 Sensitivity Analysis

The decrease of efficiency is assumed to be the effect of the decreasing molecular speed ratio rather than the decrease in density, but the effects are both contributing to the efficiency decrease. To investigate the influence of these two parameters, a sensitivity analysis is performed subsequently.

Under varying atmospheric conditions, changes in density, temperature, and particle velocity occur. However, particle velocity ranges from $v_{\max} = 7814\,\mathrm{m/s}$ to $v_{\min} = 7755\,\mathrm{m/s}$ and this variation is expected to have a negligible effect. An initial analysis, considering a velocity change from 150 km to 250 km, supported this conclusion, and the velocity effect will therefore be neglected in the subsequent analysis. As discussed earlier, the thermal velocity (as defined by Eq. (5)), and consequently temperature, is expected to have the most significant impact on intake efficiency due to changes in the molecular speed ratio. Therefore, the following analysis focuses on the effects of temperature and density changes.

Figure 11 shows the results of the sensitivity analysis of density and temperature for $l_{\mathrm{In}} = 1000\,\mathrm{mm}$ under moderate solar activity conditions. The blue solid line represents the particle flux and efficiency presented previously for moderate solar activity conditions, see Fig. 8. The red dashed line shows the results of keeping the density constant at the density of 150 km and varying only the temperature according to the changes at different altitudes for moderate solar conditions. The yellow dotted line

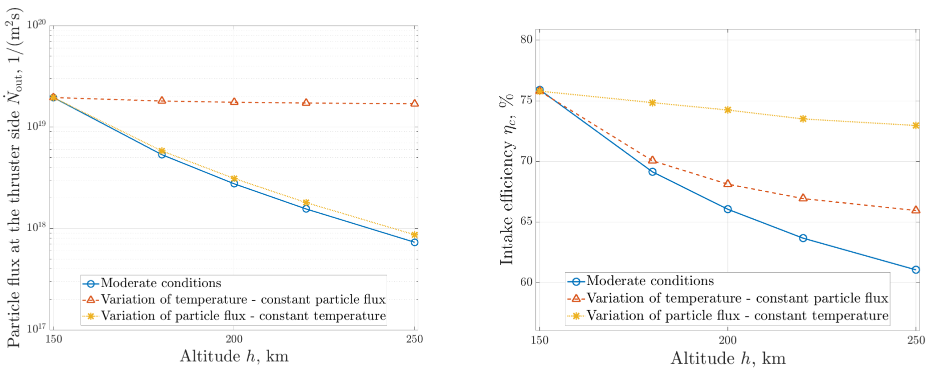

(a) Particle flux at the thruster side at the beginning of the DC over altitude

(b) Intake efficiency over altitude

Fig. 11 Sensitivity analysis of density and temperature for $l_{\mathrm{In}} = 1000\,\mathrm{mm}$ under moderate solar activity conditions shows the opposite scenario of varying the density while keeping the temperature constant with respect to the 150 km moderate solar activity case.

The left side of the graph (a) shows the particle flux at the intake outlet, indicating that the particle density significantly affects and completely dominates the number density at the outlet. Consequently, the pressure and mass flow rate follow the same trend.

The right side of Fig. 11 (b) illustrates the intake efficiency η_c, revealing a more dominant influence of particle temperature. While varying density results in only a 3% decrease in efficiency, varying temperature reduces efficiency by 10%. This confirms the initial assumption that the primary factor contributing to the decrease in efficiency is the thermal velocity of the particles. This shows that the intake efficiency is, consequently, highly dependent on the molecular speed ratio and the angle of the particle trajectory, and therefore the particles can not be assumed to act as a collimated beam. It clearly indicates that the hyperthermal assumption is not valid for VLEO flow and that the thermal velocity of the particles must be considered in future VLEO simulations of ABEP intakes.

However, the data also show that the parabolic shape, selected based on the hyperthermal assumption, still outperforms a diffuse intake in most cases, making it the preferred intake.

4.5 Efficiency Dependence on Molecular Speed Ratio

The sensitivity analysis shows a significant influence of the thermal velocity v_{th}, which is proportional to the square root of the temperature. Since the square root of the temperature increases with altitude at a rate faster than the bulk velocity of the particles, the VLEO domain experiences a decrease in molecular speed ratio with increasing altitude. This trend is already illustrated in Fig. 6 (b), which shows the molecular speed ratios for each species at different altitudes.

In order to demonstrate the direct dependence of the efficiency on the molecular speed ratio, the molecular speed ratio was averaged over the particle density and plotted against efficiency. This relationship is shown in Fig. 12.

It can be seen, that there is a nearly linear relationship between efficiency and average molecular speed ratio. The highest efficiencies are obtained at the highest molecular speed ratios, where the influence of thermal velocity is minimized. In addition, the relationship is significantly affected by the intake length, with shorter intakes showing greater efficiency.

For an intake length of 1000 mm a notable drop in efficiency occurs between altitudes of 150 km and 180 km. This drop doesn't follow the linear relationship of the molecular speed ratio and efficiency, but is continued after the drop with the same slope. This effect does not occur for simulation data with lengths of 500 mm and 1500 mm and is not further investigated at this time.

The results demonstrate that the molecular speed ratio should not be neglected as it plays a critical role in the design of ABEP intakes.

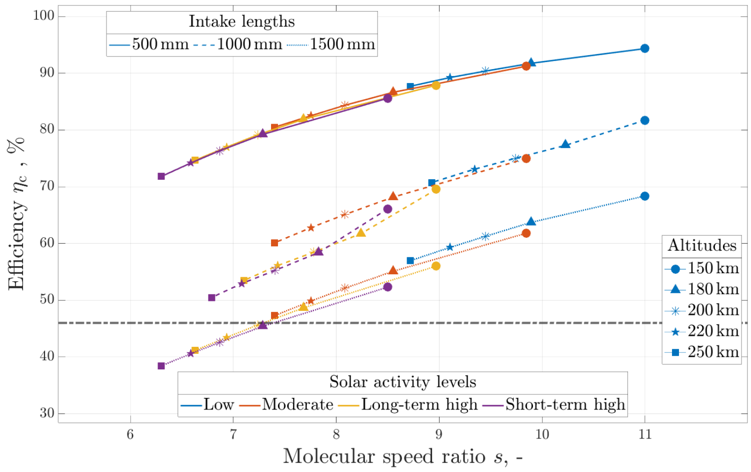

Fig. 12 Intake efficiency over molecular speed ratio s for different altitudes, solar activity levels and intake length, with the black line showing the current limit for diffuse intakes

4.6 Considering the Specularity Assumption

As mentioned earlier, all previous simulations were conducted under the assumption of 100% specularity, an idealized assumption that has not yet been achieved in practical applications. Additional simulations were performed for varying levels of specularity ranging from 50% to 100% to evaluate the robustness of this assumption and investigate the combined effect of solar activity and surface interaction behavior. If the assumption of 100% specularity is found to be inaccurate, it may be necessary to reconsider the use of the Maxwell model and explore alternatives, such as the CLL model. However, in the absence of specific material constants for the CLL coefficients, the authors argue that the current study's use of the Maxwell model with a specularity range of 50% to 100% is sufficient. Future work, when suitable material constants for the CLL model are available, may necessitate its implementation.

The simulation results for the collection efficiency of different level of specularities are presented in Fig. 13. In contrast to earlier figures, different line styles are used to distinguish between solar activity levels.

The efficiency decreases significantly as specularity reduces, falling below the efficiency of diffuse intakes at specularities below 70% across nearly all investigated altitudes. For optimal operation of a specular intake, a minimum specularity of 80% is required. To achieve superior performance at all investigated altitudes, a specularity greater than 90% is necessary.

Figure 14 shows the relative changes in efficiency at different specularity levels for various solar activity ratios, compared to low solar activity conditions. The efficiency ratio remains nearly constant across all altitudes and solar activity levels, regardless of specularity. For very low specularities and high solar activity, the ratio begins to decrease, which must be taken into account. However, in the relevant range where specularity exceeds 80%, the efficiency ratio remains stable. Therefore, we conclude

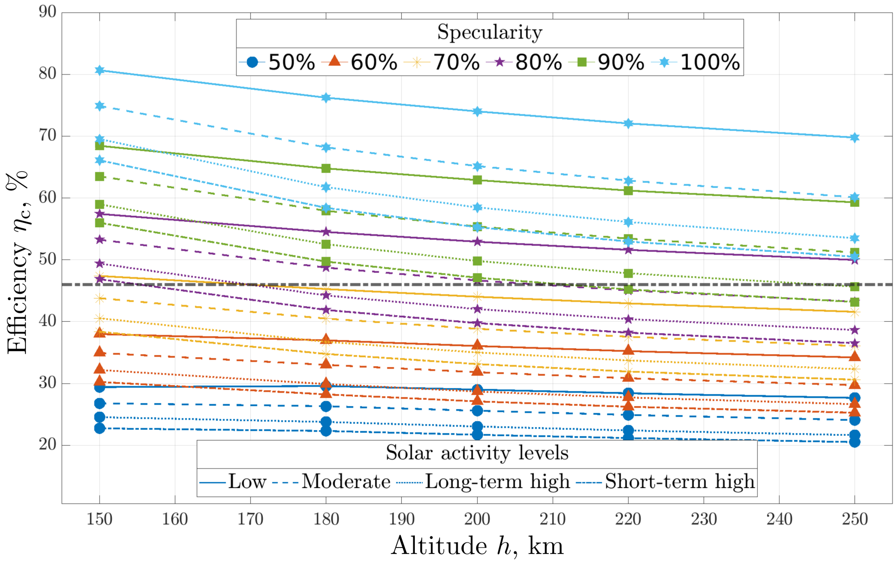

Fig. 13 Influence of different levels of specularity of the intake material and different solar activity levels on the intake efficiency, with the black line showing the current limit for diffuse intakes

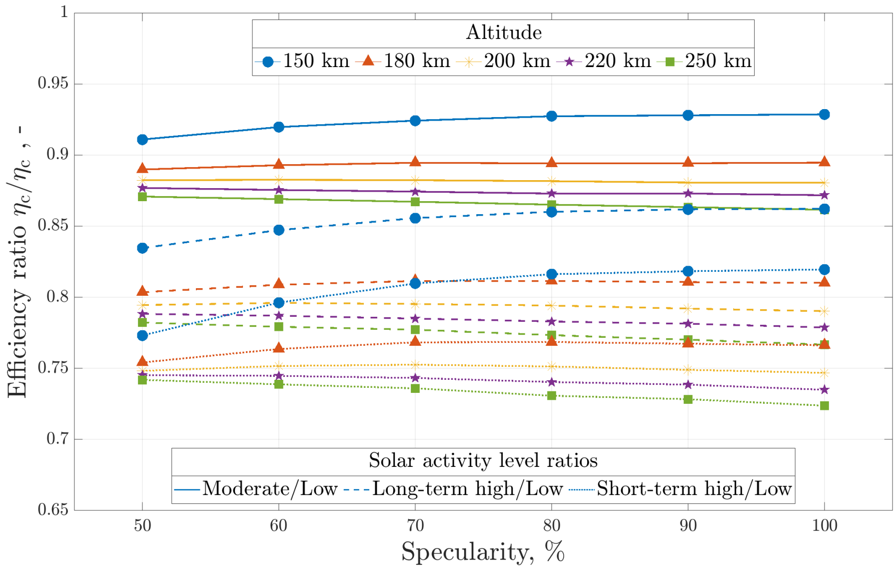

Fig. 14 Change of efficiency ratio relative to low solar activity conditions over different specularity levels

that the results presented in this paper can be extrapolated to other specularity levels through simple interpolation, without compromising accuracy.

In addition to the effect of specularity on intake efficiency, its impact on ignition pressure shall also be considered. Figure 15 illustrates the mean pressure variation

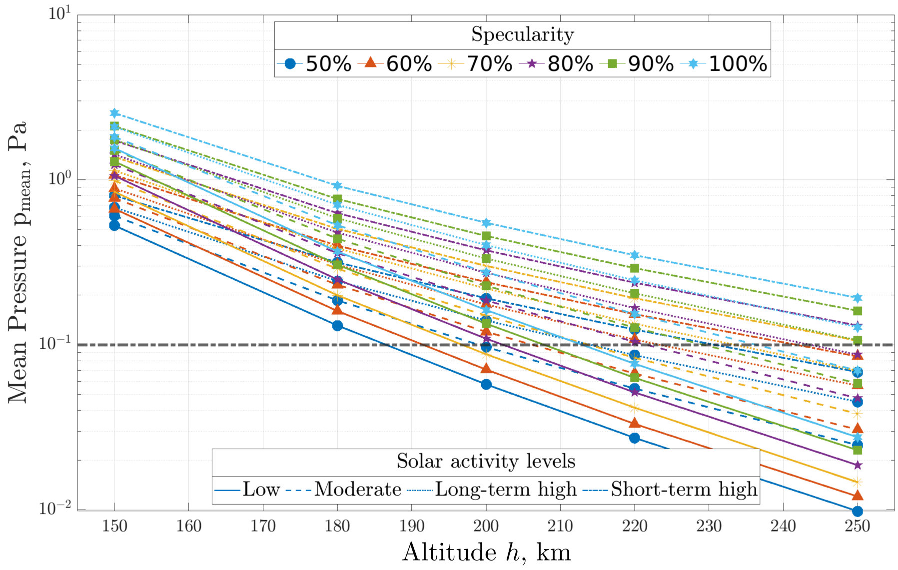

Fig. 15 Influence of different levels of specularity of the intake material and solar activity levels on the mean pressure inside the DC (p_{mean}). The black line represents the current ignition pressure, achieved by the RF Helicon-based plasma thruster [3].

at different solar activity levels and specularity assumptions, across varying altitudes. The ignition pressure (tested and reproduced so far) previously defined as 0.1 Pa [3], is represented by the black dashed line. However, as previously discussed, it is possible that the required ignition pressure may be lower upon further testing validation.

The data indicates that a decrease in specularity, leads to a reduction in mean pressure inside the DC, causing it to fall below 0.1 Pa at higher altitudes. For future mission concepts, this suggests that as the material degrades, the orbit may need to be limited to lower altitudes where ignition pressure can still be maintained. However, solar activity has a greater impact on pressure than specularity.

Higher specularity leads to improved efficiencies and pressures, highlighting the importance of preserving specularity throughout the mission. Various approaches, such as the use of specialized coatings and novel intake materials, are being explored to develop highly specular intakes.

5 Conclusion

This detailed numerical simulation study provides an insight into the complex dynamics of ABEP intake systems and provides critical knowledge of their performance under different atmospheric conditions and intake configurations. Through careful analysis and interpretation of the simulation results, several key findings emerge.

The first result of the simulations is that the effect of the solar activity level on intake efficiency is strong. It is assumed, that this trend results from the increased atmospheric temperature at different solar activities, which results in a higher thermal velocity and therefore different angles in the particle trajectories and a deviation from the bulk velocity. This can be also observed by taking a look at the molecular speed ratio of the different species over different altitudes, showing that the assumption of hyperthermal flow is not valid in the VLEO range. This is later analyzed in more detail during the sensitivity analysis, where a strong dependency between efficiency and molecular speed ratio can be shown over different solar activity levels and altitudes for the same geometry. This underlines the need to consider thermal velocities in the design and operation of ABEP intake systems.

The second result is, that the influence of intake length plays a crucial role for the design as well. The above mentioned effect is emphasized for larger intake lengths, which makes a longer specular intake less efficient. Considering results over different altitudes show, that the operation at higher altitudes results in a decrease in efficiency for all possible configurations, as the temperature is increased.

Furthermore, when considering the pressure for all conditions tested, the RF Helicon thruster ignition pressure, set in this paper, is reached for most, but not all, conditions. As mentioned above, the ignition pressure could be lower, as some experiments were conducted at a lower pressure. This limit of 0.1 Pa is validated and serves as a comparison metric in this paper. In addition, it is crucial to determine whether the mean pressure or the maximum pressure is determining the ignition, as this will influence the feasible altitudes for different atmospheric conditions.

Given these findings, a variable altitude strategy is recommended. During periods of lower solar activity, lower drag allows operation at lower altitudes. Conversely, during periods of higher solar activity, it is advisable to operate at higher altitudes, with the ignition pressure being achievable even at these higher altitudes.

Finally, it is demonstrated that assuming 100% specularity and adjusting for lower specularities can be done without sacrificing accuracy, as the relative changes over efficiency vs altitude stay constant for different specularity levels.

In summary, the results of this study provide guidance for the design, optimization and operational planning of future ABEP intake systems. By considering the complex interactions between atmospheric conditions, intake configurations and system performance metrics, engineers and researchers can develop more robust and efficient ABEP systems.

Acknowledgments

This work is funded by the Deutsche Forschungsgemeinschaft project number 516238647 - SFB1667/1, named Advancing Technologies of Very Low Altitude Satellites (ATLAS). Part of the work is also supported by the Ram-CLEP project with the name "Technology Enhancement of Atmosphere-Breathing Cathode-Less Electric Propulsion" and has received funding from ESA under the ITT AO/1-10597/20/NL/MG. The statements and conclusions outlined above reflects only the authors' view and the Deutsche Forschungsgemeinschaft or ESA are not responsible for any use that may be made of the information it contains.

References

[1] Papavramidis, K., Skalden, J., Souhair, N., Herdrich, G., Maier, P., Klinkner,

S., Fugmann, M., Traub, C., Fasoulas, S., Romano, F., Chan, Y.: Development Activities for the RF Helicon-based Plasma Thruster: Thrust Measurement and B-dot Probe Set-up. In: 37th International Electric Propulsion Conference (IEPC) Nr. 167, IEPC-2024-435 (2022)

[2] Herdrich, G., Papavramidis, K., Maier, P., García-Almiñana, D., Rodríguez Donaire, S., Sureda Anfres, M.: Platform and System Design Study of a VLEO Satellite Platform using the IRS RF Helicon-based Plasma Thruster. In: Proceedings of the 73rd International Astronautical Congress, IAC-22-C4.9.1, pp. 1–15 (2022). International Astronautical Federation

[3] Herdrich, G., Papavramidis, K., Maier, P., Skalden, J., Hild, F., Beyer, J., Pfeiffer, M., Fugmann, M., Klinker, S., Fasoulas, S., Souhair, N.: System Design Study of a VLEO Satellite Platform using the IRS RF Helicon-Based Plasma Thruster. Acta Astronautica **215**, 245–259 (2024)

[4] Nishiyama, K.: Air Breathing Ion Engine Concept. In: 54th International Astronautical Congress of the International Astronautical Federation, the International Academy of Astronautics, and the International Institute of Space Law, p. 4 (2003)

[5] Jackson, S.W., Marshall, R.: Conceptual Design of an Air-Breathing Electric Thruster for CubeSat Applications. Journal of Spacecraft and Rockets **55**(3), 632–639 (2018)

[6] Romano, F., Espinosa-Orozco, J., Pfeiffer, M., Herdrich, G., Crisp, N.H., Roberts, P., Holmes, B., Edmondson, S., Haigh, S., Livadiotti, S., A, M.-R.: Intake Design for an Atmosphere-Breathing Electric Propulsion System (ABEP). Acta Astronautica **187**, 225–235 (2021)

[7] Fujita, K.: Air-Intake Performance Estimation of Air-Breathing Ion Engines. Nippon Kikai Gakkai Ronbunshu B Hen(Transactions of the Japan Society of Mechanical Engineers Part B)(Japan) **16**(12), 3038–3044 (2004)

[8] Fujita, K.: Air Intake Performance of Air Breathing Ion Engines. Japan Society of Aeronautical Space Sciences **52**(610), 514–521 (2005)

[9] Hisamoto, Y., Nishiyama, K., Kuninaka, H.: Development Status of Atomic Oxygen Simulator for Air Breathing Ion Engine. In: 32nd Intern. Electric Propulsion Conference (IEPC), IEPC-2011-294 (2011)

[10] Hisamoto, Y., Nishiyama, K., Kuninaka, H.: Design of Air Intake for Air Breathing Ion Engine. In: 63rd International Astronautical Congress, Naples, Italy (2012)

[11] Tagawa, M., Yokota, K., Nishiyama, K., Kuninaka, H., Yoshizawa, Y., Yamamoto, D., Tsuboi, T.: Experimental Study of Air Breathing Ion Engine using Laser

Detonation Beam Source. Journal of Propulsion and Power **29**(3), 501–506 (2013)

[12] Di Cara, D., Del Amo, J.G., Santovincenzo, A., Dominguez, B.C., Arcioni, M., Caldwell, A., Roma, I.: RAM Electric Propulsion for Low Earth Orbit Operation: an ESA Study. In: 30th International Electric Propulsion Conference, IEPC-2007-162 (2007)

[13] Hohman, K.: Atmoshperic Breathing Electric Thruster for Planetary Exploration, Busek 288. Final Report, Natick, MA (2012)

[14] Barral, S., Cifali, G., Albertoni, R., Andrenucci, M., Walpot, L.: Conceptual Design of an Air-Breathing Electric Propulsion System. In: 34th International Electric Propulsion Conference and 6th Nanosatellite Symposium, IEPC-2015-271/ISTS-2015-b-271 (2015)

[15] Cifali, G., Andrenussi, T., Giannetti, V., Leoprini, A., Rossodivita, A., Andrenucci, M., Barral, S., Longo, J., Walpot, L.: Experimental Validation of a RAM-EP Concept Based on Hall-Effect Thruster. 34th international electric propulsion conference (IEPC), IEPC-2017-377 (2016)

[16] Andreussi, T., Cifali, G., Giannetti, V., Piragino, A., Ferrato, E., Rossodivita, A., Andrenucci, M., Longo, J., Walpot, L.: Development and Experimental Validation of a Hall Effect Thruster RAM-EP Concept. In: 35th International Electric Propulsion Conference (IEPC), SP2018_00431 (2017)

[17] Andreussi, T., Ferrato, E., Giannetti, V., Piragino, A., Paissoni, C.A., Cifali, G., Andrenucci, M.: Development Status and way forward of SITAELs Air-Breathing Electric Propulsion Engine. In: AIAA Propulsion and Energy 2019 Forum, p. 3995 (2019)

[18] Ferrato, E., Giannetti, V., Piragino, A., Andrenucci, M., Andreussi, T., Paissoni, C.A.: Development Roadmap of SITAELs RAM-EP system. In: 36th International Electric Propulsion Conference (IEPC), IEPC-2019-886 (2019)

[19] Parodi, P., Le Quang, D., Bariselli, F., Boccelli, S., Alsalihi, Z., Magin, T.: Study of a Collector-Intake System for VLEO Air-Breathing Platforms. In: International Conference on Flight Vehicles, Aerothermodynamics and Re-entry Missions and Engineering (FAR), Monopoli, Italy, vol. 10 (2019)

[20] Fedele, A., Carannante, S., Grassi, M., Savino, R.: Aerodynamic Control System for a Deployable Re-entry Capsule. Acta Astronautica **181**, 707–716 (2021)

[21] Li, Y., Chen, X., Li, D., Xiao, Y., Dai, P., Gong, C.: Design and Analysis of Vacuum Air-Intake Device used in Air-Breathing Electric Propulsion. Vacuum **120**, 89–95 (2015)

[22] Romano, F., Binder, T., Herdrich, G., Fasoulas, S., Schönherr, T.: Air-Intake

Design Investigation for an Air-Breathing Electric Propulsion System. International Symposium on Space Technology and Science (2015)

[23] Romano, F., Binder, T., Herdrich, G., Fasoulas, S., Schönherr, T.: Intake Design for an Atmosphere-Breathing Electric Propulsion System. Space Propulsion, SP2016 3124981 (2016)

[24] Kanev, S., Petukhov, V., Popov, G., Khartov, S.: Electro-Rocket Ramjet Thruster for Compensating the Aerodynamic Drag of a Low-Orbit Spacecraft. Russian Aeronautics (Iz VUZ) **58**, 286–291 (2015)

[25] Erofeev, A., Nikiforov, A., Popov, G., Suvorov, M., Syrin, S., Khartov, S.: Air-Breathing Ramjet Electric Propulsion for Controlling Low-Orbit Spacecraft Motion to Compensate for Aerodynamic Drag. Solar System Research **51**, 639–645 (2017)

[26] Erofeev, A.I.: Air Intake in the Transient Regime of Rarefied Gas Flow. TsAGI Science Journal **49**(2) (2018)

[27] Marov, M.Y., Filatyev, A.: Integrated Studies of Electric Propulsion Engines during Flights in the Earths Ionosphere. Cosmic Research **56**, 123–129 (2018)

[28] Filatyev, A.S., Yanova, O.V.: The Control Optimization of Low-orbit Spacecraft with Electric Ramjet. Acta Astronautica **158**, 23–31 (2019)

[29] Golikov, A., Nosachev, L., Skvortsov, V., Filatyev, A., Padalitsa, D.: Spacecraft with Air-Breathing Electric Propulsion as the future Ultra-Speed Aircraft. In: Proceedings of the International Astronautical Congress (IAC), IAC-20, C4, 6, 8, X59643 (2020)

[30] Feng, K.: Investigation of a Novel Atmosphere-Breathing Electric Propulsion Platform and Intake (2023)

[31] Zheng, P., Jianjun, W., Zhang, Y., Bixuan, C., Yuanzheng, Z.: An Atmosphere-Breathing Propulsion System using Inductively Coupled Plasma Source. Chinese Journal of Aeronautics **36**(5), 223–238 (2023)

[32] Sannino, A., Pessina, V., Savino, R., Schein, J.: Design and performances of intake for atmosphere-breathing electric propulsion systems with the direct simulation Monte Carlo method. Physics of Fluids **37**(2) (2025)

[33] Wu, J., Zheng, P., Zhang, Y., Tang, H.: Recent Development of Intake Devices for Atmosphere-Breathing Electric Propulsion System. Progress in Aerospace Sciences **133** (2022)

[34] Cercignani, C., Lampis, M.: Kinetic models for gas-surface interactions. Transport theory and statistical physics **1**(2), 101–114 (1971)

[35] Prieto, D.M., Graziano, B.P., Roberts, P.C.: Spacecraft Drag Modelling. Progress in Aerospace Sciences **64**, 56–65 (2014)

[36] Livadiotti, S., Crisp, N.H., Roberts, P.C.E., Worrall, S.D., Oiko, V.T.A., Edmondson, S., Haigh, S.J., Huyton, C., Smith, K.L., Sinpetru, L.A., Holmes, B.E.A., Becedas, J., Domnguez, R.M., Caas, V., Christensen, S., Mlgaard, A., Nielsen, J., Bisgaard, M., Chan, Y.-A., Herdrich, G.H., Romano, F., Fasoulas, S., Traub, C., Garcia-Almiana, D., Rodriguez-Donaire, S., Sureda, M., Kataria, D., Belkouchi, B., Conte, A., Perez, J.S., Villain, R., Outlaw, R.: A Review of Gas-Surface Interaction Models for Orbital Aerodynamics Applications. Progress in Aerospace Sciences **119** (2020)

[37] Murray, V.J., Pilinski, M.D., Smoll Jr, E.J., Qian, M., Minton, T.K., Madzunkov, S.M., Darrach, M.R.: Gas-Surface Scattering Dynamics Applied to Concentration of Gases for Mass Spectrometry in Tenuous Atmospheres. The Journal of Physical Chemistry C **121**(14), 7903–7922 (2017)

[38] Herdrich, G., Auweter-Kurtz, M., Löhle, S., Pidan, S., Laux, T.: Oxidation Behaviour of SiC-based Thermal Protection System Materials using newly developed Probe Techniques. Journal of Spacecraft and Rockets **42**(5), 817–824 (2005)

[39] Massuti-Ballester, B., Herdrich, G., Friess, M.: Oxidation of PM1000 and C/C-SiC exposed to Highly Dissociated Oxygen and Nitrogen Flows. Journal of the European Ceramic Society **40**(6), 2306–2316 (2020)

[40] Picone, J., Hedin, A., Drob, D.P., Aikin, A.: NRLMSISE-00 Empirical Model of the Atmosphere: Statistical Comparisons and Scientific Issues. Journal of Geophysical Research: Space Physics **107**(A12), 15 (2002)

[41] ISO-14222: Space Environment (natural and artificial) Earth Upper Atmosphere. Technical report (2013)

[42] ECSS-E-10-04C: Space Environment. Technical report, ESA Publications Division (2020)

[43] Bird, G.A.: Molecular Gas Dynamics and the Direct Simulation of Gas Flows (1994)

[44] Fasoulas, S., Munz, C.-D., Pfeiffer, M., Beyer, J., Binder, T., Copplestone, S., Mirza, A., Nizenkov, P., Ortwein, P., Reschke, W.: Combining Particle-In-Cell and Direct Simulation Monte Carlo for the Simulation of Reactive Plasma Flows. Physics of Fluids **31**(7) (2019)

[45] Pfeiffer, M., Mirza, A., Fasoulas, S.: A grid-independent particle pairing strategy for DSMC. Journal of Computational Physics **246**, 28–36 (2013)

[46] Shiwei, Z., Jin, H., Zhijun, Z.: Computer Simulation of Positional Beaming Effect of Molecular Flow in Straight Cylindrical Pipeline by Monte Carlo Method. In: 2008 International Conference on Computer Science and Information Technology, pp. 486–491 (2008)